New Journal of Physics

CrossMark

PAPER

Coulomb time delays in high harmonic generation

Lisa Torlina[1] and Olga Smirnova[1,2]

[1] Max Born Institute for Nonlinear Optics and Short Pulse Spectroscopy, Max-Born-Strasse 2 A, D-12489 Berlin, Germany
[2] Technische Universität Berlin, Ernst-Ruska-Gebäude, Hardenbergstr. 36A, D-10623, Berlin, Germany

E-mail: olga.smirnova@mbi-berlin.de

Abstract

Measuring the time it takes to remove an electron from an atom or molecule during photoionization has been the focus of a number of recent experiments using newly developed attosecond spectroscopies. The interpretation of such measurements, however, depends critically on the measurement protocol and the specific observables available in each experiment. One such protocol relies on high harmonic generation. In this paper, we derive rigorous and general expressions for ionisation and recombination times in high harmonic generation experiments. We show that these times are different from, but related to, ionisation times measured in photoelectron spectroscopy: that is, those obtained using the attosecond streak camera, RABBITT and attoclock methods. We then proceed to use the analytical *R*-matrix theory to calculate these times and compare them with experimental values.

1. Introduction

The problem of time-resolving the removal of an electron during photoionization and studying the time delays associated with this process is an intriguing one [1]. Besides the fundamental implications for our understanding of atom-light interaction, such measurements have the capacity to serve as a sensitive probe of multielectron dynamics [2, 3] and have an important role to play in calibrating attosecond recollision-based pump-probe experiments [4].

Indeed, recent experimental developments—including the attosecond streak camera [5], the attoclock [6, 7], attosecond transient absorption [8], RABBIT [9–11] and high harmonic spectroscopy [4, 12, 13]—have made it possible to measure ionisation times down to the level of tens of attoseconds, both in the one-photon [5, 9, 10] and multi-photon regimes [4, 6–8, 12–14]. In each case, however, a thorough theoretical understanding [15–21] of the underlying physics has been crucial to correctly interpret the experimental results. To do so, it is necessary to formulate a connection between the classical concept of time, the quantum wavefunction and the experimental observables. The times obtained are inherently very sensitive to the way in which this is done.

In the one-photon case, the theoretical basis for doing so is now well-established (e.g. see [1, 22]). Ionisation is thought of as a half-scattering process and time delays are defined in terms of the Eisenbud–Wigner–Smith (EWS) time [23, 24]: the derivative of the scattering phase-shift of the photoelectron with respect to its energy,

$$\Delta t_{\mathrm{WS}} = -\frac{\mathrm{d}\phi_f^s}{\mathrm{d}E_k}. \tag{1}$$

In the multiphoton regime, however, the situation is notably less straightforward. If we think of ionisation as a tunnelling process, we are presented with a number of different possible definitions for the tunnelling time, and it is not clear from the outset which is the 'correct' time to use (e.g. see [25–27]). What's more, the use of any of these definitions in the context of strong field ionisation necessarily restricts us to the tunnelling limit. It is not clear a-priori how to take non-adiabatic effects into account or how to investigate the effect on time delays as we move towards the few-photon limit [28].

Alternatively, the concept of ionisation time arises in another way within certain analytical approaches to strong field ionisation. These include the widely used and broadly successful strong field approximation (SFA)—which we use here as an umbrella term for the related work of Keldysh [29], Perelomov *et al* [30, 31], Faisal [32] and Reiss [33]—as well as the more recently developed analytical *R*-matrix (ARM) method [34–39]. The latter is a fully quantum theory that is able to accurately describe the long-range Coulomb interaction between the outgoing electron and the core—the absence of which is the main limitation of the SFA. In each of these approaches, it is necessary to integrate over a time variable that describes the instant at which the bound electron first interacts with the field. In analytical approaches, this integral is typically evaluated using the saddle point method, and the real part of the complex saddle point solution, $t_i = \mathrm{Re}[t_s]$, is interpreted as the most probable time of ionisation—that is, the time at which the electron appears in the continuum. The concept of saddle point time as ionisation time also features in the Coulomb-corrected SFA approach [40, 41] (see also recent review [42] and recent update of the theory [43]), which takes the SFA ionisation amplitude as its starting point.

Q1

Recently, the above idea was applied to analyse [3] the results of the attoclock experiment [6, 7, 14], the basic premise of which relies on using short pulses of circularly or nearly circularly polarised light to induce ionisation and deflect electrons in different directions, depending on their time of ionisation. Using ARM to describe this experimental setup and applying saddle point analysis, it was possible to derive an expression for ionisation time as a function of the angle and momentum (θ, p) at which the photoelectron is observed [3]:

$$t_i = t_i^0(\theta, p) + \Delta t^C(\theta, p). \tag{2}$$

The first term, $t_i^0 = \theta/\omega + \Delta t^{\mathrm{env}}(\theta, p)$, is the SFA saddle point result, accurate in the limit of short-range potentials (where ω is the angular frequency of the laser field and $\Delta t^{\mathrm{env}}(\theta, p)$ is a small correction due to the shape of the pulse envelope). The second term Δt^C is an additional delay that comes about due to the long-range electron-core interaction. It takes the form

$$\Delta t^C = -\frac{\partial \phi^C}{\partial I_p}, \tag{3}$$

where ϕ^C is the phase accumulated by the outgoing electron due to its interaction with the ionic core and I_p is the ionisation potential of the bound state from which the electron escaped [3]. Expression (3) has also been derived within the ARM method in [37]. Applying this relationship to analyse the results of *ab initio* numerical experiments, it was shown that accounting for the delay Δt^C was vital to correctly interpret experimental results and reconstruct the ionisation time [3].

In fact, equation (3), which we can think of as the delay accumulated in a long-range potential compared to a short-range potential, coincides with an expression for ionisation delay derived in an entirely different way. In [28], the idea of the Larmor clock—originally proposed in the context of tunnelling times—was applied to ionisation. It was shown to reduce to the EWS time in the single-photon limit and reproduce equation (3) in the strong field regime. Thus, the different definitions for times are not unrelated: there is a link between the saddle point-based ionisation time, the Larmor tunnelling time and the EWS single-photon delay.

The attoclock, however, is not the only means by which ionisation times can be measured in the strong field regime. Two-colour high harmonic spectroscopy experiments offer another elegant and powerful approach to this problem, using a weak probe pulse to perturb the ionisation dynamics in a controlled way [4]. In light of this, a number of questions naturally arise. Are the times measured in HHG the same as those by the attoclock? If not, how are they related? How does the electron-core interaction imprint itself on the ionisation and recombination times in this case?

Here, we address these questions by extending the saddle point analysis discussed above to HHG. After briefly reviewing the basic approaches for describing time in HHG in section 2, we present a general analysis that incorporates electron-core interaction in section 3, and discuss how such a calculation can be implemented in practice using ARM in section 4. In section 5, we present results of this calculation and compare our findings to times reconstructed from two-colour high harmonic spectroscopy experiments. Finally, we discuss the results and analyse the magnitude of Coulomb corrections to times in section 6. Section 7 concludes the work.

2. Ionisation and recombination times in HHG: a brief overview

2.1. The classical model

The simplest theoretical description of ionisation time in the context of HHG comes from the classical model, which describes the process in terms of three steps: tunnel ionisation, classical propagation in the continuum and recombination. In the standard classical model [44] (see also pertinent [45–48]), electron-core interaction is neglected during the classical propagation step, and it is assumed that the electron starts its continuum motion with a velocity of zero. If we also assume that recombination occurs when the electron returns to its starting point and relate its kinetic energy at this instant to the energy of the emitted photon, we obtain the following

three equations:

$$\mathbf{v}(t_i) = 0, \tag{4}$$

$$\int_{t_i}^{t_r} \mathbf{v}(t)\,\mathrm{d}t = 0, \tag{5}$$

$$\frac{1}{2}v(t_r)^2 = E_\omega - I_p, \tag{6}$$

where $\mathbf{v}(t) = \mathbf{p} + \mathbf{A}(t)$ is the electron velocity, $\mathbf{A}$ is the vector potential that describes the laser field $\mathcal{E} = -\frac{\partial \mathbf{A}}{\partial t}$, and $E_\omega = N\omega$ is the energy of the emitted photon.

For any given photon energy E_ω, the above equations can be solved for the ionisation time t_i, the recombination time t_r and the canonical momentum $\mathbf{p}$. As such, we can associate an ionisation and recombination time to each harmonic number: this defines the mapping between experimental observable and time in this case. However, although excellent as a first approximation, this model is clearly rather crude. It artificially matches a quantum mechanical description of the ionisation step with classical propagation, assumes very simple initial conditions for the electron's continuum motion and ignores the influence of the positively charged ionic core. It is not surprising, therefore, that a comparison of the above predictions with times obtained in high harmonic spectroscopy experiments revealed a notable discrepancy [4].

2.2. The SFA

As mentioned in the introduction, the SFA offers a more sophisticated quantum approach to the problem of time in strong field ionisation, which is based on saddle point analysis. In essence, the key approximation of the SFA is to neglect the interaction between the electron and its parent ion after the instant ionisation or, equivalently, to assume that the core potential is short range. Doing so, the induced dipole can be expressed as [49]:

$$\mathbf{D}(N\omega) = -\mathrm{i} \int \mathrm{d}t \int \mathrm{d}\mathbf{p} \int \mathrm{d}t'\, P(t', t, \mathbf{p})\, \mathrm{e}^{\mathrm{i}E_\omega t}\, \mathrm{e}^{-\mathrm{i}I_p(t-t')}\, \mathrm{e}^{-\mathrm{i}S_V(t,t',\mathbf{p})}, \tag{7}$$

where S_V is the Volkov phase

$$S_V = \frac{1}{2} \int_t^{t'} v^2(\tau)\,\mathrm{d}\tau, \tag{8}$$

and P is a prefactor that varies relatively slowly. The times t' and t over which we integrate can be associated with ionisation and recombination respectively.

The presence of a large phase, which leads to rapid oscillations of the integrand, makes it possible to evaluate the above integral using the saddle point method. It tells us that the integral will be accumulated predominantly in the vicinity of points where the derivative of the phase vanishes, which are defined by the saddle point equations [49, 50]:

$$\frac{\partial S_V}{\partial t'} = I_p, \tag{9}$$

$$\frac{\partial S_V}{\partial \mathbf{p}} = 0, \tag{10}$$

$$\frac{\partial S_V}{\partial t} = E_\omega - I_p. \tag{11}$$

We shall denote the solutions to these equations by t_ι^0, $\mathbf{p}_s^0$, t_ρ^0.

In fact, it is easy to check that equations (10) and (11) coincide exactly with equations (5) and (6) from the classical model, while equation (9) is a modified version of equation (4): $v^2(t') = -2I_p$. The latter, in fact, gives rise to a key difference between the two descriptions. Whereas the solutions in the classical model are fully real, their counterparts in SFA are complex in general (see e.g. discussion in [51, 52]). Nevertheless, as mentioned in the introduction, the real parts of the saddle point solutions come with an interpretation. We can associate $t_i^0 = \mathrm{Re}[t_\iota^0]$, $\mathbf{p}^0 = \mathrm{Re}[\mathbf{p}_s^0]$ and $t_r^0 = \mathrm{Re}[t_\rho^0]$ with the time of ionisation, canonical momentum and time of recombination respectively. For short-range potentials, this interpretation is particularly transparent (e.g. see discussion in [3]). As such, equations (9)–(11) again define a mapping between time and harmonic number, albeit a somewhat different one.

Using this model, it was shown that agreement with times reconstructed from high harmonic spectroscopy experiments is notably improved [4]. However, what both the classical model and the SFA have in common is the neglect of the long-range electron-core interaction throughout the electron's motion in the continuum. In the context of the attoclock, we have seen that this is not sufficient: ignoring the influence of the core potential on saddle point solutions leads to qualitatively and quantitatively incorrect results [3]. Motivated by this, let us now consider how the above solutions are modified if we allow for an electron-core interaction term.

3. Influence of electron-core interaction on times in HHG: a general analysis

It was shown in [34] that, within ARM, the SFA expression for the ionisation amplitude—the analogous quantity to the induced dipole given by equation (7)—is modified by the addition of a Coulomb term e^{-iW_C}. This term accounts for the effect of the long-range interaction between the outgoing electron and its parent ion. Let us now consider what a term of this nature would imply for times in HHG.

In particular, suppose that the integral in equation (7) now includes some additional factor $e^{-iF(t',t,\mathbf{p})}$, which takes electron-core interaction into account. Although ARM can provide us with an explicit expression for F, to which we shall return in section 4, we shall keep the analysis general for the time being. We assume only that F is small compared to S_V and allow it to be complex in general. The real part of F then specifies the phase associated with the electron-core interaction, which we shall denote by $\phi = \mathrm{Re}[F]$.

The saddle point equations (9)–(11) are then modified as follows

$$\frac{\partial S_V}{\partial t'} + \frac{\partial F}{\partial t'} = I_p, \tag{12}$$

$$\frac{\partial S_V}{\partial \mathbf{p}} + \frac{\partial F}{\partial \mathbf{p}} = 0, \tag{13}$$

$$\frac{\partial S_V}{\partial t} + \frac{\partial F}{\partial t} = E_\omega - I_p, \tag{14}$$

and since F is small compared to S_V, we can search for solutions of the form $(t_\iota^0 + \Delta t_\iota,\ p_s^0 + \Delta p_s,\ t_\rho^0 + \Delta t_\rho)$, where $(t_\iota^0,\ p_s^0,\ t_\rho^0)$ satisfy equations (9)–(11). Expanding about the SFA saddle points, keeping only first order terms in F, and using the chain rule to rewrite the derivatives, we arrive at the following result (see appendix A):

$$\Delta t_\iota = -\frac{\partial F}{\partial I_p} - \frac{\partial F}{\partial E_\omega}, \tag{15}$$

$$\Delta t_\rho = -\frac{\partial F}{\partial E_\omega}. \tag{16}$$

In general, since F is complex, these corrections will also be complex. However, as before, we can assign an interpretation to their real parts: $\Delta t_i = \mathrm{Re}[\Delta t_\iota]$ and $\Delta t_r = \mathrm{Re}[\Delta t_\rho]$ encode the delays due to the electron-core interaction imprinted upon ionisation and recombination times respectively:

$$\Delta t_i = -\frac{\partial \phi}{\partial I_p} - \frac{\partial \phi}{\partial E_\omega}, \tag{17}$$

$$\Delta t_r = -\frac{\partial \phi}{\partial E_\omega}. \tag{18}$$

There are a few things worth noting about the above results. First, notice that the expression for the correction to the recombination time, $\Delta t_r = -\partial\phi/\partial E_\omega$, is reminiscent of the EWS time given by equation (1). Indeed, we can understand this if we recall that recombination is simply single-photon ionisation run in reverse. Varying with respect to the photon energy is directly equivalent to varying with respect to the kinetic energy of the recombining electron. Second, note that the correction to ionisation time in HHG, $\Delta t_i = -\partial\phi/\partial I_p - \partial\phi/\partial E_\omega$, has an extra term compared to its counterpart in strong field ionisation given by equation (3). Subtracting the above expressions for Δt_r and Δt_i yields

$$\Delta t_r - \Delta t_i = \Delta(t_r - t_i) = \frac{\partial \phi}{\partial I_p}. \tag{19}$$

In other words, the derivative of the phase with respect to the ionisation potential in HHG tells us how much more (or less) time the electron will spend in the continuum before it recombines, as a consequence of electron-core interaction.

4. Coulomb corrections in HHG using ARM

Keeping the function F unspecified, this is as far as we can go. If we want to determine the corresponding time delays in practice, we must evaluate F explicitly. Luckily, this is precisely what ARM allows us to do.

In particular, it was shown in [34] that if we apply ARM to strong field ionisation, e^{-iF} is replaced by $e^{-iW_C^{SFI}}$, where

$$W_C^{\mathrm{SFI}}(\mathbf{p},\, T) = \int_{t_\kappa}^{T} \mathrm{d}t'\; U(\mathbf{r}_s(\mathbf{p},\, t')). \tag{20}$$

Here, W_C^{SFI} is the electron action associated with the Coulomb-laser coupling [53, 54], $\mathbf{p}$ is the electron momentum measured at the detector, T is the time of observation, $U(\mathbf{r})$ is the core potential and $\mathbf{r}_s$ is the Coulomb-free electron trajectory,

$$\mathbf{r}_s(\mathbf{p},\, t') = \int_{t_\iota}^{t'} (\mathbf{p} + \mathbf{A}(t''))\mathrm{d}t''. \tag{21}$$

The lower limit of the integral in equation (20), $t_\kappa = t_\iota - \mathrm{i}/\kappa^2$, is determined by the boundary-matching procedure for the outgoing electron [34, 37].

Indeed, this boundary matching was crucial. It made it possible to smoothly merge the asymptotic tail of the bound electron wavefunction with the quasiclassical wavefunction of the escaping electron driven by the laser field, and allowed us to avoid using W_C^{SFI} too close to the ionic core, beyond its range of applicability. In strong field ionisation, it was only necessary to carry out this matching once, when the electron departed from its parent atom or molecule. In HHG, on the other hand, we know that we must also account for the recombination step, when the electron returns to the core. This makes it necessary to perform the matching procedure once more, to connect the phase due to Coulomb-laser coupling accumulated between ionisation and recombination to the field-free continuum solution for the returning electron. Effectively, doing so will tell us the correct endpoint t_{end} to use in place of the observation time T in the upper integration limit of the HHG counterpart to equation (20).

Fortunately, an equivalent boundary-matching problem has already been solved. In [17], single photon ionisation in the presence of a probing infra-red field was analysed in the context of the attosecond streak camera. There, a matching argument was used to show that the effective starting point for an electron trajectory with initial velocity v_0 is given by

$$r_0(v_0) = \frac{1}{v_0\, a(v_0)}, \tag{22}$$

where

$$a(v_0) = 2\mathrm{e}^{-2\gamma_{\mathrm{E}}}\mathrm{e}^{2\xi(v_0)}, \tag{23}$$

γ_{E} is Euler's constant and

$$\xi(v_0) = \sum_{n=1}^{\infty} \frac{1}{n}\left[1 - v_0 n \arctan\left(\frac{1}{v_0 n}\right)\right]. \tag{24}$$

Noting that recombination in HHG is simply the reverse of this process (that is, the emission, rather than absorption, of a photon in the presence of an infra-red field), we can apply this result directly to determine the boundary-matched endpoint t_{end}. In particular, we now think of r_0 as the end point of our electron trajectory and set $r_0 = r_s(t_{\mathrm{end}})$. The corresponding velocity v_0 is the velocity at recombination,

$$v_0 = v_{\mathrm{r}} = \sqrt{2(E_\omega - I_p)}. \tag{25}$$

For any given photon energy E_ω, we then have

$$r_0(v_{\mathrm{r}}) = r_s(t_{\mathrm{end}}) = \int_{t_\iota(E_\omega)}^{t_{\mathrm{end}}} (p_s(E_\omega) + A(t))\, \mathrm{d}t, \tag{26}$$

which can be used to solve for t_{end}, using equations (22)–(25) to evaluate $r_0(v_{\mathrm{r}})$.

In doing so, it should be noted that $r_s(t)$ is complex in general for real times, whereas r_0 is always real. Consequently, in order to satisfy the above equation, we must allow t_{end} to be complex as well. This tells us that, in contrast to ionisation, our integral for W_C will no longer end on the real axis: both start and end points are now complex. The generalisation, however, is straightforward. When describing Coulomb effects in strong field ionisation, the integration contour was chosen in two parts: first, down from t_κ to $\mathrm{Re}[t_\iota] = t_{\mathrm{i}}$ on the real axis, and then along the real axis up to time T [34, 38]. These two legs were interpreted in terms of tunnel ionisation and the electron's motion in the continuum respectively, following PPT [31]. For HHG, we simply add a third leg: down from $\mathrm{Re}[t_{\mathrm{end}}]$ on the real axis to t_{end} (see figure 1).

We note that, in general, the interpretation of the real part of the complex saddle point as the ionisation time is not connected to a certain choice of the integration contour. Analytic properties of the integrand in W_C, of course, make it possible to deform the contour considerably without influencing the result of the integration. However, in contrast to the contour, the saddle point time itself is unique and well-defined: it has a real and an imaginary part. In fact, the real part of the saddle point can be directly probed experimentally using the attoclock setup [3], as discussed in section 1. In the long wavelength limit, the attoclock observable (the so-called offset angle) is simply equal to the real part of the saddle point time multiplied by the angular frequency [28]. What's
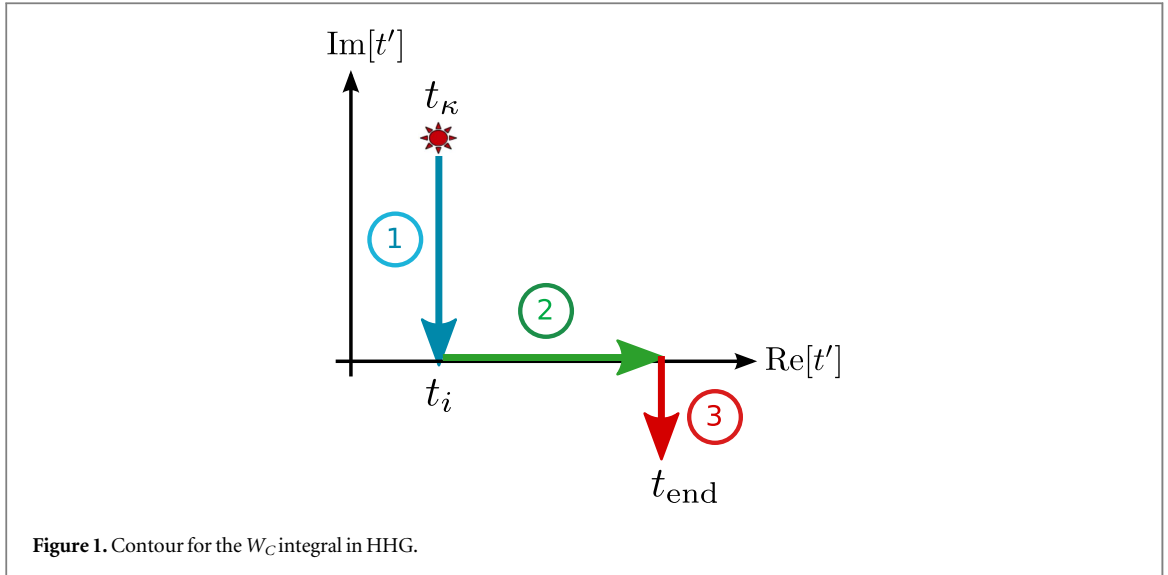
Figure 1. Contour for the W_C integral in HHG.

more, the expression for the ionisation time we obtain from the real part of the saddle point coincides with that derived using an alternative method in [28]. The latter method uses neither the concept of tunnelling nor trajectories, nor does it rely on saddle point analysis, yet the result for the ionisation time remains the same.

Having determined the correct integration endpoint t_{end} by boundary matching, it is straightforward to write down the HHG counterpart to equation (20). There are only two major changes we need to make: (1) the momentum at the detector $\mathbf{p}$ should be replaced by the saddle point solution $\mathbf{p}_s(E_\omega)$, and (2) the observation time T should be replaced by the time t_{end}. That is,

$$W_C^{\mathrm{HHG}}(E_\omega) = \int_{t_\kappa}^{t_{end}} \mathrm{d}t' \, U(\mathbf{r}_s(E_\omega, t')), \tag{27}$$

where

$$\mathbf{r}_s(E_\omega, t') = \int_{t_i(E_\omega)}^{t'} (\mathbf{p}_s(E_\omega) + \mathbf{A}(t'')) \mathrm{d}t''. \tag{28}$$

We can readily determine the value of $\mathbf{p}_s(E_\omega)$ from equations (9)–(11).

5. Results: Coulomb time delays in HHG

Having determined t_{end} and chosen a contour, we have all the ingredients we need in order to evaluate the correction W_C as given by equation (27). In itself, this tells us the first order effects on HHG spectra due to the long-range electron-core interaction. However, as we saw in section 3, we need one further step to learn about times: we must differentiate the Coulomb phase $\phi = \mathrm{Re}[W_C]$ with respect to I_p and E_ω to find the corrections to the saddle point solutions, as given by equations (17) and (18). In practice, this can be done numerically by evaluating W_C for two or more closely spaced values of I_p, E_ω.

We shall now compare these results with times reconstructed from high harmonic spectroscopy measurements, originally published in [4]. In essence, in addition to the fundamental field responsible for HHG, the experiment uses a weak probe field to deflect electrons laterally during their motion in the continuum. By varying the delay of the probe field with respect to the fundamental and observing the associated variation in harmonic signal, it is possible to determine the time at which ionisation and recombination occurred. The details of the associated reconstruction procedure are described in [4] (see also SI of [4]) and analysed in detail in [19]. For the benefit of the reader, we also briefly outline the main idea of the procedure in appendix B.

Figure 2 shows the results for the helium atom. The ionisation and recombination times obtained using ARM (blue lines) are compared to SFA (black lines), the classical model (grey lines) and times reconstructed from high harmonic spectroscopy experiments (pink and green dots, see [4]). Note that, as discussed in appendix B, the experiment could only determine the difference between ionisation and recombination times, and their dependence on harmonic number: the results are valid up to an overall additive constant. To plot absolute times, we calibrate the experiment by shifting all ionisation and recombination times by a fixed amount until we achieve the best possible fit with the recombination times predicted by our models (as figure 2 shows, there is relatively little variation in recombination times between different models, so this is unambiguous).

Figure 2. Ionisation and recombination times predicted using the classical model (grey lines), SFA (black lines) and ARM (blue lines) compared with times reconstructed from high harmonic spectroscopy experiments (pink and green dots, see [4]) for helium atoms at $\lambda = 800$ nm and $I \approx 3.8 \times 10^{14}$ W cm^{-2}.
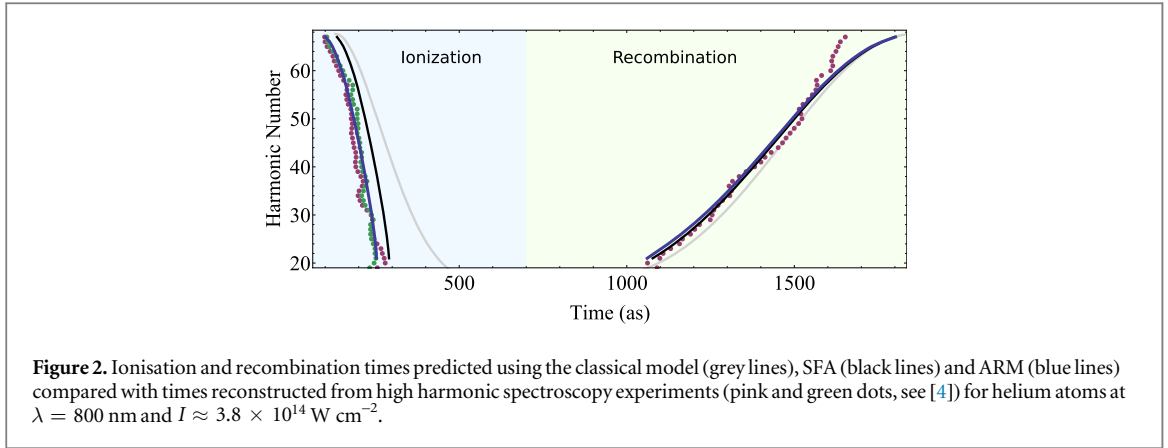
Compared to the SFA, we find that the corrected ionisation times in ARM are shifted to earlier values. This effect has only a weak dependence on harmonic number: the shift varies between ~33 and ~37 attoseconds, decreasing slightly with *N*. The recombination times are notably less affected overall, though they display a stronger dependence on the harmonic number. The shift in this case is between ~5 and ~19 attoseconds, again decreasing with *N*. Putting these two facts together, we see that the total amount of time the electron spends in the continuum (given by $\partial\phi/\partial I_p$) increases by ~18–28 attoseconds. The relative size of these corrections and their dependence on harmonic number is analysed further in section 6.

Comparing our results with times reconstructed from high harmonic spectroscopy measurements, we find that ARM offers a notable improvement over the SFA, where electron-core interaction was neglected. Although the corrections to ionisation and recombination times are only of the order of tens of attoseconds, they are nevertheless clearly within the resolution of current state-of-the-art HHG experiments.

We note that our method also makes it possible to analyse the Coulomb corrections to imaginary times. The results of doing so are presented in [13], where imaginary ionisation times where reconstructed from experimental measurements.

6. Discussion: how can we understand the size of the corrections?

If we consider the results presented in the previous section, it is natural to ask why the shift in ionisation times due to the electron-core interaction is notably larger than the shift in recombination times. Can we estimate the relative size of these two corrections and understand their dependence on harmonic number? What are the small parameters associated with each of them?

Referring back to equations (17) and (18) from section 3, it is clear that to answer these questions we must look more closely at the two partial derivatives

$$\Delta t_1 \equiv -\frac{\partial\phi}{\partial I_p}, \tag{29}$$

$$\Delta t_2 \equiv -\frac{\partial\phi}{\partial E_\omega}, \tag{30}$$

of which Δt_i and Δt_r are composed. Let us analyse each of these in turn.

First, consider $\Delta t_1 = \partial\phi/\partial I_p$. We recall from equation (3) in section 1 that this coincides with Δt^C, the first order correction to the saddle point time in strong field ionisation relative to the SFA result. To obtain a simple analytical expression for the small parameter associated with this term, let us now take the tunnelling limit. In this limit, the imaginary part of the SFA saddle point t_i^0 is given by $\tau = \sqrt{2I_p}/\mathcal{E}(t_i)$ where $\mathcal{E}(t_i)$ is the magnitude of the laser field at the moment of ionisation: this is the well-known Keldysh tunnelling time. The real part of the saddle point can be chosen to be zero. At the same time, it is possible to show that, in the tunnelling limit, the correction Δt^C due to the electron-core interaction takes the value $\Delta t_i^{SF} \approx Z/I_p^{3/2}$, where Z is the charge of the core (see derivation in [36, 37]). Its imaginary component vanishes to first order in this limit. Taking the ratio of the norms of these two complex quantities, we obtain

$$\zeta_1 = \frac{|\Delta t_1|}{|t_i^0|} = \frac{Z\mathcal{E}(t_i)}{\sqrt{2}\,I_p^2} = \frac{n^*}{2\mathrm{Im}S^{SF}}\frac{2^{5/2}}{3}, \tag{31}$$

where $n^* = Z/I_p^{1/2}$ is the effective principal quantum number of a given quantum state and $\mathrm{Im}S^{SFA}$ is the imaginary part of the electron action associated with the electron's dynamics in the laser field only. The quantum

number n^* characterises the action of the electron in the bound state, while S^{SFA} characterises the action of the electron driven by the laser field. As long as the action due to the laser-driven dynamics exceeds the action in the ground state—which is usually the case in strong field ionisation—the ratio ζ_1 will remain small. Indeed, this condition is essentially equivalent to the condition for applicability of most Coulomb-corrected SFA theories.

Let us now turn our attention to the second correction term $\Delta t_2 = -\partial\phi/\partial E_\omega$. This term is the analogue of the well-known Wigner–Smith ionisation time given by equation (1), albeit the phase ϕ here is not the field-free scattering phase, but incorporates the effects of the laser field and describes Coulomb-laser coupling. To obtain a small parameter associated with this term, let us consider a ratio of velocities: $\zeta_2 = \Delta q/v_r$, where Δq is the shift of electron momentum due to Coulomb-laser coupling, and v_r is the velocity of the electron at the moment of recombination, as given by equation (25). Using the expression for Δq from [54], we find

$$\zeta_2 = \frac{Z\mathcal{E}(t_r)}{v_r|2^{3/2}(E_\omega - I_p)^{3/2}|)} = \frac{Z\mathcal{E}(t_r)}{v_r^4}, \tag{32}$$

where $\mathcal{E}(t_r)$ is the magnitude of the laser field at the recombination time.

If we now compare expressions (31) and (32) for our two small parameters, we notice that they have a similar structure. Both are of the form

$$\zeta \propto \frac{Z\mathcal{E}}{v^4}. \tag{33}$$

For ζ_1, v is the electron velocity of the bound state $v_b = \sqrt{2I_p}$ and $\mathcal{E}$ is the magnitude of the laser field at the moment of ionisation. For ζ_2, we have the velocity of the returning electron v_r and the laser field at the moment of recombination.

What can this tell us about the relative size of Δt_i and Δt_r? In HHG, we know that the velocity of the returning electron is larger than that associated with the bound state. At the same time, the instantaneous value of the laser field is larger at ionisation than at recombination, or they are comparable, for majority of electron trajectories (except those corresponding to low harmonic numbers). Based on the small parameters above, this suggests that Δt_2 should be smaller than Δt_1, which, in turn, helps explain why corrections to ionisation times, given by $\Delta t_1 + \Delta t_2$, are notably larger than corrections to recombination times, determined by Δt_2 alone.

The expressions for ζ_1 and ζ_2 may also shed light on the dependence of Δt_i and Δt_r on harmonic number. Higher harmonics are associated with higher recombination velocities v_r and lower values of the instantaneous field $\mathcal{E}(t_r)$, which, via ζ_2, would explain why corrections to recombination times decrease with harmonic number. Since, conversely, the instantaneous field at ionisation $\mathcal{E}(t_i)$ displays a slow increase with harmonic number, while v_b is fixed, we would expect that Δt_1 grows with N. Putting these two facts, we can understand the observed values of Δt_i. Its behaviour is governed by an interplay of both terms and—since Δt_2 decreases faster than Δt_1 increases—this would explain the slow decrease of Δt_i with N observed in our results.

Finally, it should be noted that both Δt_1 and Δt_2 are inherently small, which can make it difficult to resolve Δt_i and Δt_r in practice. In particular, these corrections have not been seen in the numerical simulations of [55].

7. Conclusions and outlook

In this paper, we have shown how ionisation and recombination times in HHG are modified when the long-range interaction between the active electron and the ionic core is taken into account. The resulting corrections are closely related to the delays in strong field and single photon ionisation respectively, though they are not identical. In particular, the expression for the ionisation delay in HHG, $\Delta t_i^{HHG} = -\partial\phi/\partial I_p - \partial\phi/\partial E_\omega$, contains an additional term compared to its counterpart in strong field ionisation, $\Delta t_i^{SFI} = -\partial\phi/\partial I_p$ (derived in [3, 28, 37]). In essence, this 'additional' ionisation delay stems from the different measurement protocols used in strong field ionisation and HHG experiments respectively. While the former detect photoelectrons, the latter detect the XUV photons that are generated when electrons return to the core. Consequently, in the case of HHG, the 'delay-line' on the way to the detector is associated not only with ionisation (which includes propagation in the continuum), but also with the recombination step, which brings with it a delay of its own.

Comparing the predictions of the ARM theory—in which the electron-core interaction is accounted for—with times measured in high harmonic spectroscopy experiments, we find that the agreement is excellent. The fit is visibly better than for the SFA, where such effects are omitted. Thus, although relatively small, we can conclude that the electron-core interaction leaves a measurable and distinct signature on times in HHG. As such, it should be taken into consideration when calibrating attosecond recollision-based pump-probe experiments and interpreting experimental data.

Acknowledgments

Appendix A. Derivation of general expression for saddle point corrections

In this section we present the derivation of equations (15), (16). To do so, it will be convenient to introduce the following vectors

$$\mathbf{s} = (t', p, t), \tag{A1}$$

$$\mathbf{s}^0 = (t_\iota^0, p_s^0, t_\rho^0), \tag{A2}$$

$$\mathbf{\Delta s} = (\Delta t_\iota, \Delta p_s, \Delta t_\rho), \tag{A3}$$

$$\mathbf{\Upsilon} = (I_p, X, E_\omega) \tag{A4}$$

and the vector-valued function

$$\mathbf{f}: \quad \mathbb{R}^3 \to \mathbb{R}^3$$
$$(I_p, X, E_\omega) \mapsto (I_p, X, E_\omega - I_p). \tag{A5}$$

The gradient ∇ will be defined as a row vector, and $\nabla_{\mathbf{s}^0} F$ will occassionally be used as shorthand for $\nabla_{\mathbf{s}} F(\mathbf{s}^0)$, where F is the function introduced in section 3.

Using this notation, the saddle point equations (12)–(14) can be expressed succinctly as

$$\nabla_{\mathbf{s}} S_V(\mathbf{s}^0 + \mathbf{\Delta s}) + \nabla_{\mathbf{s}} F(\mathbf{s}^0 + \mathbf{\Delta s}) = \mathbf{f}(\mathbf{\Upsilon}), \tag{A6}$$

while their analogues in the SFA become

$$\nabla_{\mathbf{s}} S_V(\mathbf{s}^0) = \mathbf{f}(\mathbf{\Upsilon}), \tag{A7}$$

where we have added a constant $X \to 0$ to the lhs of the second saddle point equation for convenience in both cases.

If we now expand the solution to equation (A6) about $\mathbf{s}^0$, we obtain (to first order in $\mathbf{\Delta s}$ and $\nabla_{\mathbf{s}} F$)

$$\nabla_{\mathbf{s}} S_V(\mathbf{s}^0) + \mathbf{\Delta s} \, [J_{\mathbf{s}}[\nabla_{\mathbf{s}} S_V](\mathbf{s}^0)]^T + \nabla_{\mathbf{s}} F(\mathbf{s}^0) = \mathbf{f}(\mathbf{\Upsilon}), \tag{A8}$$

where $J_{\mathbf{s}}$ is the Jacobian with derivatives taken with respect to $\mathbf{s}$. Using equation (A7) and the fact that the Jacobian of a gradient is the Hessian, we have

$$\mathbf{\Delta s} \, [H_{\mathbf{s}}[S_V](\mathbf{s}^0)]^T = -\nabla_{\mathbf{s}} F(\mathbf{s}^0). \tag{A9}$$

Since the Hessian is symmetric and invertible (in this case), we can rewrite this as

$$\mathbf{\Delta s} = -\nabla_{\mathbf{s}^0} F \, [H_{\mathbf{s}^0}[S_V]]^{-1}. \tag{A10}$$

In principle, if we could evaluate $\nabla_{\mathbf{s}^0} F$, we would be done. However, we do not have direct control over the value of the complex saddle point $\mathbf{s}$ when we do the calculation numerically, which makes this a difficult quantity to work with. Instead, what we can do is vary the parameters $\mathbf{\Upsilon}$ and see how F changes as a result—this makes it possible to evaluate $\nabla_{\mathbf{\Upsilon}} F$ numerically. With this in mind, we would like to rewrite equation (A10) in terms of $\nabla_{\mathbf{\Upsilon}} F$ instead of $\nabla_{\mathbf{s}} F$.

To do so, we note that equation (A7) establishes a functional relationship between $\mathbf{s}^0$ and $\mathbf{\Upsilon}$. In principle, we could solve this equation to find $\mathbf{s}^0(\mathbf{\Upsilon})$. Taking the gradient of F with respect to $\mathbf{\Upsilon}$ and applying the chain rule gives

$$\nabla_{\mathbf{\Upsilon}} F(\mathbf{s}^0(\mathbf{\Upsilon})) = \nabla_{\mathbf{s}} F(\mathbf{s}^0) \, J_{\mathbf{\Upsilon}}[\mathbf{s}^0(\mathbf{\Upsilon})], \tag{A11}$$

so

$$\nabla_{\mathbf{s}^0} F = \nabla_{\mathbf{\Upsilon}} F \, [J_{\mathbf{\Upsilon}}[\mathbf{s}^0]]^{-1}. \tag{A12}$$

We now need only evaluate the Jacobian $J_{\mathbf{\Upsilon}}[\mathbf{s}^0]$. To do so, let us differentiate both sides of the SFA saddle point equation equation (A7) with respect to $\mathbf{\Upsilon}$:

$$J_{\mathbf{\Upsilon}}[\nabla_{\mathbf{s}} S_V(\mathbf{s}^0(\mathbf{\Upsilon}))] = J_{\mathbf{\Upsilon}}[\mathbf{f}(\mathbf{\Upsilon})]. \tag{A13}$$

Applying the chain rule again, we can rewrite this as

$$J_{\mathbf{s}}[\nabla_{\mathbf{s}} S_V(\mathbf{s}^0)] \, J_{\Upsilon}[\mathbf{s}^0(\Upsilon)] = J_{\Upsilon}[\mathbf{f}(\Upsilon)], \tag{A14}$$

and so (again making use of the fact that the Jacobian of a gradient is the Hessian),

$$J_{\Upsilon}[\mathbf{s}^0] = H_{\mathbf{s}^0}[S_V]^{-1} \, J_{\Upsilon}[\mathbf{f}]. \tag{A15}$$

Taking the inverse and substituting this into equation (A12) gives

$$\nabla_{\mathbf{s}^0} F = \nabla_{\Upsilon} F \, [J_{\Upsilon}[\mathbf{f}]]^{-1} \, H_{\mathbf{s}^0}[S_V]. \tag{A16}$$

Finally, this allows us to rewrite equation (A10) as

$$\Delta\mathbf{s} = -\nabla_{\Upsilon} F \, [J_{\Upsilon}[\mathbf{f}]]^{-1} \, H_{\mathbf{s}^0}[S_V] \, [H_{\mathbf{s}^0}[S_V]]^{-1}, \tag{A17}$$

which simplifies to

$$\Delta\mathbf{s} = -\nabla_{\Upsilon} F \, [J_{\Upsilon}\mathbf{f}]^{-1}. \tag{A18}$$

In our case, $J_{\Upsilon}\mathbf{f}$ is very simple:

$$J_{\Upsilon}\mathbf{f} = \begin{pmatrix} 1 & 0 & 0 \\ 0 & 1 & 0 \\ -1 & 0 & 1 \end{pmatrix}, \tag{A19}$$

and

$$[J_{\Upsilon}\mathbf{f}]^{-1} = \begin{pmatrix} 1 & 0 & 0 \\ 0 & 1 & 0 \\ 1 & 0 & 1 \end{pmatrix}. \tag{A20}$$

This allows us to write down a solution for $\Delta\mathbf{s}$ in terms of $\nabla_{\Upsilon} F$:

$$\Delta t_s = -\frac{\partial F}{\partial I_p} - \frac{\partial F}{\partial E_{\omega}}, \tag{A21}$$

$$\Delta p_s = -\frac{\partial F}{\partial X}, \tag{A22}$$

$$\Delta t_{\mathrm{r}} = -\frac{\partial F}{\partial E_{\omega}}. \tag{A23}$$

Appendix B. Reconstruction procedure for times in high harmonic spectroscopy experiments

Suppose HHG is driven by a strong laser field with fundamental frequency ω, described by the vector potential $A_{\omega}(t) = \vec{e}_x A_0 \sin(\omega t)$. To probe the associated ionisation times, let us also apply an additional perturbative control field with frequency 2ω, given by $A_{2\omega}(t) = \vec{e}_y A_0 \sin(2\omega t + \alpha)$, which is phase locked to the fundamental field and polarised in an orthogonal direction. This field will effectively 'kick' the electron in a lateral direction when it leaves its bound atomic state and exits from the tunnelling barrier at the ionisation time t_{i}. The magnitude and sign of this kick is controlled by α, the relative phase between the two fields, referred to as the 'two-colour delay'.

As we vary α, we find that the HHG yield is modulated. In particular, the harmonic signal attains its maximum value when the lateral kick is equal to zero or, in other words, when the electron displacement between ionisation and recombination is minimised. To good approximation, this occurs when the vector potential of the control field at the moment of ionisation is close to zero: that is, $A_{2\omega}(t_{\mathrm{i}}) = \vec{e}_y A_0 \sin(2\omega t_{\mathrm{i}} + \alpha_{\max}) \approx 0$ if $\alpha_{\max}$ is the two-colour delay at which the harmonic signal is maximised. This, in turn, gives us a relationship between the observed $\alpha_{\max}$ and the ionisation time t_{i}: $|t_{\mathrm{i}}| \approx \alpha_{\max}/\omega$. In the full reconstruction, corrections accounting for the kick during tunnelling are also included.

Note that the second harmonic field breaks the symmetry in electron dynamics between the two consecutive laser half cycles, which leads to the generation of even harmonics. This asymmetry is greatest at those values of α where the lateral velocity of the electron upon recombination is largest. In practice, recombination times are reconstructed following the maximum HHG signal for even harmonics, as suggested and performed in [4] and augumented in [55] by including complex (rather than real) SFA recollision times.

Note also that the experiment can only reconstruct (i) the delay between ionisation and recombination time, (ii) the dependence of the ionisation and recombination times on harmonic energy. In order to determine the absolute values of ionisation and recombination times in HHG, it is necessary to calibrate $\alpha_{\max}$. We do this by

shifting all times by a fixed amount until we obtain the best fit with the recombination times predicted by our models. This is a consistent way to proceed since recombination times do not differ considerably between models.

References

Q2

[1] Pazourek R, Nagele S and Burgdörfer J 2015 Attosecond chronoscopy of photoemission *Rev. Mod. Phys.* **87** 765
[2] Carette T, Dahlström J, Argenti L and Lindroth E 2013 Multiconfigurational hartree-fock close-coupling ansatz: application to the argon photoionization cross section and delays *Phys. Rev.* A **87** 023420
[3] Torlina L *et al* 2015 Interpreting attoclock measurements of tunnelling times *Nat. Phys.* **11** 503–8
[4] Shafir D, Soifer H, Bruner B D, Dagan M, Mairesse Y, Patchkovskii S, Ivanov M Y, Smirnova O and Dudovich N 2012 Resolving the time when an electron exits a tunnelling barrier *Nature* **485** 343–6
[5] Schultze M *et al* 2010 Delay in photoemission *Science* **328** 1658–62
[6] Eckle P, Smolarski M, Schlup P, Biegert J, Staudte A, Schöffler M, Muller H G, Dörner R and Keller U 2008 Attosecond angular streaking *Nat. Phys.* **4** 565–70
[7] Eckle P, Pfeiffer A N, Cirelli C and Staudte A 2008 Attosecond ionization and tunneling delay time measurements in helium *Science* **322** 1525–9
[8] Goulielmakis E *et al* 2010 Real-time observation of valence electron motion *Nature* **466** 739–43
[9] Klünder K *et al* 2011 Probing single-photon ionization on the attosecond time scale *Phys. Rev. Lett.* **106** 143002
[10] Guenot D *et al* 2012 Photoemission-time-delay measurements and calculations close to the 3 s-ionization-cross-section minimum in ar *Phys. Rev.* A **85** 053424
[11] Gunot D *et al* 2014 Measurements of relative photoemission time delays in noble gas atoms *J. Phys. B: At. Mol. Opt. Phys.* **47** 245602
[12] Soifer H, Dagan M, Shafir D, Bruner B D, Ivanov M Y, Serbinenko V, Barth I, Smirnova O and Dudovich N 2013 Spatio-spectral analysis of ionization times in high-harmonic generation *Chem. Phys.* **414** 176–83
[13] Pedatzur O *et al* 2015 Attosecond tunnelling interferometry *Nat. Phys.* **11** 815–9
[14] Pfeiffer A N, Cirelli C, Smolarski M, Dimitrovski D, Abu-Samha M, Madsen L B and Keller U 2012 Attoclock reveals natural coordinates of the laser-induced tunnelling current flow in atoms *Nat. Phys.* **8** 76–80
[15] Shvetsov-Shilovski N I, Dimitrovski D and Madsen L B 2012 Ionization in elliptically polarized pulses: multielectron polarization effects and asymmetry of photoelectron momentum distributions *Phys. Rev.* A **85** 023428
[16] Dahlström J, Guénot D, Klünder K, Gisselbrecht M, Mauritsson J, L'Huillier A, Maquet A and Taïeb R 2013 Theory of attosecond delays in laser-assisted photoionization *Chem. Phys.* **414** 53–64
[17] Ivanov M and Smirnova O 2011 How accurate is the attosecond streak camera? *Phys. Rev. Lett.* **107** 213605
[18] Nagele S, Pazourek R, Feist J, Doblhoff-Dier K, Lemell C, Tksi K and Burgdrfer J 2011 Time-resolved photoemission by attosecond streaking: extraction of time information *J. Phys. B: At. Mol. Opt. Phys.* **44** 081001
[19] Serbinenko V and Smirnova O 2013 Multidimensional high harmonic spectroscopy: a semi-classical perspective on measuring multielectron rearrangement upon ionization *J. Phys. B: At. Mol. Opt. Phys.* **46** 171001
[20] Maquet A, Caillat J and Taïeb R 2014 Attosecond delays in photoionization: time and quantum mechanics *J. Phys. B: At. Mol. Opt. Phys.* **47** 204004
[21] Gaillac R, Vacher M, Maquet A, Taïeb R and Caillat J 2016 Attosecond photoemission dynamics encoded in real-valued continuum wave functions *Phys. Rev.* A **93** 013410
[22] Dahlström J M, L'Huillier A and Maquet A 2012 Introduction to attosecond delays in photoionization *J. Phys. B: At. Mol. Opt. Phys.* **45** 183001
[23] Wigner E 1955 Lower limit for the energy derivative of the scattering phase shift *Phys. Rev.* **98** 145–7
[24] Smith F T 1960 Lifetime matrix in collision theory *Phys. Rev.* **118** 349–56
[25] Landauer R and Martin T 1994 Barrier interaction time in tunneling *Rev. Mod. Phys.* **66** 217–28
[26] de Carvalho C A A and Nussenzveig H M 2002 Time delay *Phys. Rep.* **364** 83–174
[27] Yamada N 2004 Unified derivation of tunneling times from decoherence functionals *Phys. Rev. Lett.* **93** 170401
[28] Kaushal J, Morales F, Torlina L, Ivanov M and Smirnova O 2015 Spinorbit Larmor clock for ionization times in one-photon and strong-field regimes *J. Phys. B: At. Mol. Opt. Phys.* **48** 234002
[29] Keldysh L V 1965 Ionization in the field of a strong electromagnetic wave *Sov. Phys.—JETP* **20** 1307–14
[30] Perelomov A M, Popov V S and Terent'ev M V 1966 Ionization of Atoms in an alternating electric field *Sov. Phys.—JETP* **23** 924–34
[31] Perelomov A M, Popov V S and Terent'ev M V 1967 Ionization of atoms in an alternating electric field: II *Sov. Phys.—JETP* **24** 207–17
[32] Faisal F H M 1973 Multiple absorption of laser photons by atoms *J. Phys. B: At. Mol. Phys.* **6** L89–92
[33] Reiss H R 1980 Effect of an intense electromagnetic field on a weakly bound system *Phys. Rev.* A **22** 1786–813
[34] Torlina L and Smirnova O 2012 Time-dependent analytical *R*-matrix approach for strong-field dynamics: I. One-electron systems *Phys. Rev.* A **86** 043408
[35] Torlina L, Ivanov M, Walters Z B and Smirnova O 2012 Time-dependent analytical *r*-matrix approach for strong-field dynamics: II. Many-electron systems *Phys. Rev.* A **86** 043409
[36] Kaushal J and Smirnova O 2013 Nonadiabatic Coulomb effects in strong-field ionization in circularly polarized laser fields *Phys. Rev.* A **88** 013421
[37] Kaushal J, Morales F and Smirnova O 2015 Opportunities for detecting ring currents using an attoclock setup *Phys. Rev.* A **92** 063405
[38] Torlina L, Kaushal J and Smirnova O 2013 Time-resolving electron-core dynamics during strong-field ionization in circularly polarized fields *Phys. Rev.* A **88** 053403
[39] Torlina L, Morales F, Muller H and Smirnova O 2014 *Ab initio* verification of the analytical *r*-matrix theory for strong field ionization *J. Phys. B: At. Mol. Opt. Phys.* **47** 204021
[40] Popruzhenko S V and Bauer D 2008 Strong field approximation for systems with Coulomb interaction *J. Mod. Opt.* **55** 2573–89
[41] Popruzhenko S V, Paulus G G and Bauer D 2008 Coulomb-corrected quantum trajectories in strong-field ionization *Phys. Rev.* A **77** 053409
[42] Popruzhenko S 2014 Keldysh theory of strong field ionization: history, applications, difficulties and perspectives *J. Phys. B: At. Mol. Opt. Phys.* **47** 204001
[43] Popruzhenko S 2014 Invariant form of Coulomb corrections in the theory of nonlinear ionization of atoms by intense laser radiation *J. Exp. Theor. Phys.* **118** 580–6

Q3

[44] Corkum P B 1993 Plasma perspective on strong field multiphoton ionization *Phys. Rev. Lett.* **71** 1994–7

[45] Schafer K, Yang B, DiMauro L and Kulander K 1993 Above threshold ionization beyond the high harmonic cutoff *Phys. Rev. Lett.* **70** 1599

[46] van Linden van den Heuvell H and Muller H 1988 *Multiphoton Processes* (*Cambridge Studies in Modern Optics* vol 8) ed S J Smith and P L Knight (Cambridge: Cambridge University Press)

[47] Corkum P, Burnett N and Brunel F 1989 Above-threshold ionization in the long-wavelength limit *Phys. Rev. Lett.* **62** 1259

[48] Kuchiev M Y 1987 Atomic antenna *Sov. J. Exp. Theor. Phys. Lett.* **45** 404

[49] Lewenstein M, Balcou P, Ivanov M Y, Lhuillier A and Corkum P B 1994 Theory of high-harmonic generation by low-frequency laser fields *Phys. Rev.* A **49** 2117

[50] Salières P *et al* 2001 Feynman's path-integral approach for intense-laser-atom interactions *Science* **292** 902–5

[51] Smirnova O and Ivanov M 2014 Multielectron high harmonic generation: simple man on a complex plane *Attosecond and XUV Physics*   Q4
(New York: Wiley) pp 201–56

[52] Smirnova O and Ivanov M Y 2013 Multielectron high harmonic generation: simple man on a complex plane arXiv:1304.2413   Q5

[53] Smirnova O, Spanner M and Ivanov M 2008 Analytical solutions for strong field-driven atomic and molecular one- and two-electron continua and applications to strong-field problems *Phys. Rev.* A **77** 033407

[54] Smirnova O, Mouritzen A S, Patchkovskii S and Ivanov M Y 2007 Coulomb-laser coupling in laser-assisted photoionization and molecular tomography *J. Phys. B: At. Mol. Opt. Phys.* **40** F197

[55] Zhao J and Lein M 2013 Determination of ionization and tunneling times in high-order harmonic generation *Phys. Rev. Lett.* **111** 043901